論文 / 著書情報
Article / Book Information

Title	Generalized response spectrum analysis based computational morphogenesis for metal gridshells with buckling-restrained braces subjected to seismic loading
Authors	Yuki Terazawa, Atsuya Niimi, Deepshikha Nair, Toru Takeuchi
Citation	Computers and Structures, Volume 275, No. 275, p. 106914
Pub. date	2023, 1

Computers and Structures 275 (2023) 106914

Contents lists available at ScienceDirect

Computers and Structures

journal homepage: www.elsevier.com/locate/compstruc

Generalized response spectrum analysis based computational morphogenesis for metal gridshells with buckling-restrained braces subjected to seismic loading

Yuki Terazawa [a,*], Atsuya Niimi [b], Deepshikha Nair [b], Toru Takeuchi [a]

[a] Tokyo Institute of Technology, Department of Architecture and Building Engineering, Ookayama 2-12-1, Meguro-ku, Tokyo 152-8550, Japan
[b] Arup, Fujimi 2-10-2, Chiyoda-ku, Tokyo 102-0071, Japan

ARTICLE INFO

Article history:
Received 24 February 2022
Accepted 2 October 2022
Available online 22 October 2022

Keywords:
Structural morphogenesis
Parametric design
Shape optimization
Gridshell
Buckling-restrained brace
Response spectrum analysis

ABSTRACT

Structural morphogenesis is widely used as a parametric tool to find an optimal structural shape of shell structures for a prescribed objective function and a given design load. However, the current optimization methods are limited to finding a geometry under only a specific static load like the dead load or an equivalent static seismic load for predefined geometrical shapes, and so can not be applied to free-form gridshells. This poses a challenge to achieving an efficient free-form shell structure in high seismic hazard areas. This paper aims to resolve this by presenting a computational morphogenesis method to obtain form-found shell structures by considering the dynamic seismic loads and the response reduction effects of seismic energy-dissipating devices using generalized response spectrum analysis. The method was applied to optimize the buckling-restrained brace layouts on target spherical metal gridshell structures with different diameter-to-height ratios. The resulting form-found structures had an efficient roof geometry, along with an efficient damper layout (to prevent member buckling and the dropout of finishing materials). Dampers were found to be more efficient if placed in the (relatively heavy) supporting structure instead of the roof, and a flattened but locally bulged roof shape proved to be the most efficient in mitigating the seismic response. The generalized response spectrum analysis significantly reduced the computation time while evaluating the displacement response with sufficient practical accuracy, although it slightly underestimates the acceleration response if compared to the conventional nonlinear response history analysis results.

1. Introduction

Structural morphogenesis [1] (also called form-finding [2]) is a forward process of finding an optimal structural geometry (e.g. a shape of shell structure) to minimize (or maximize) objective functions while satisfying structural, architectural, and constructional constraints under a given design loading. As physical and computational morphogenesis were once exclusive to experts, with the advent of three-dimensional computer-aided design software (3D CAD) with visual programing languages (like Rhinoceros + Grass hopper [3] and Autodesk's Dynamo [4]), they have now become common among designers of all levels. However, the methods currently available in the commercial software may be used to find an optimal geometry form found considering only static loads, the most common being the dead loads. Although the geometry or shape of a structure is one of the most influencing design parameters for seismic performance, the dynamic response demand under seismic load (i.e. seismic response) is not explicitly considered in these form-finding methods. In areas of high seismic hazard (e.g. United States, New Zealand, Italy, Turkey, China, Taiwan, Philippines, and Japan), the seismic response is critical for design because the truss members of the metal gridshells may experience post-buckling ductile fracture [5–7] causing global collapse during a major earthquake event. This inhibits the realization of visually-appealing free-form gridshells (like the National Museum in the Netherland [2] and the British Museum in the United Kingdom [2]) in such countries. Therefore, structural morphogenesis methods considering both the dead load and the seismic loads are strongly desirable for such high seismic hazard areas. Furthermore, in countries such as Japan, the decision to incorporate energy-dissipation devices (dampers) in supporting structures e.g. [5,8–10] to mitigate not only the seismic response of supporting structures but also seismic input amplified by supporting

* Corresponding author.
E-mail address: terazawa.y.aa@m.titech.ac.jp (Y. Terazawa).

https://doi.org/10.1016/j.compstruc.2022.106914
0045-7949/

structures to the roof is widely adopted for regular spatial structures (i.e. arenas, stadiums, and halls). Thus, it is crucial to include this response reduction effect by dampers in the seismic optimization process.

There is limited literature available on structural morphogenesis methods to obtain efficient shell structures against seismic loads. Marmo et al. [12] proposed a Thrust Network Analysis [11] considering equivalent static seismic loads. Michiel and Adriaenssens et al. [13–15] also proposed a form-finding method considering seismic loads on masonry concrete shells. In the reference [13], a Dynamic Relaxation Method was proposed considering a simple cyclic horizontal load and was used to determine the optimal thickness of the assigned material. In the reference [14], an application of this method to an example arch structure composed of masonry blocks with differential thicknesses was demonstrated. In the reference [15], a form-finding method was proposed for corrugated shell structures under dead loads and an equivalent static seismic load by using a funicular polygon that was iteratively updated based on graphic statics. The study also demonstrated the significant seismic response of the form-found structure by nonlinear pushover analysis. Tomasello and Adriaenssens et al. [16] performed response history analysis and modal analysis on the form-found shell structures (obtained considering only dead loads) to investigate the dynamic characteristics, and discussed the obtained funicular polygon under seismic loads. Shigeta and Ogawa et al. [17] proposed a method to (computationally) optimize the shape and member stiffness distributions for single-layer reticulated shells under dead loads or equivalent static seismic loads and compared the buckling loads and their deformation capacities by using linear buckling analysis. Nascimbene[18] proposed a method to optimize fiber-reinforced composite structures under dead loads and equivalent static wind loads though and analyzed the performance of the optimization results. However, in all of the existing methods, as the dynamic seismic loads are not explicitly considered and are first simplified as equivalent static loads for the specified shell geometry, the complex vibration characteristics and seismic responses of shell structures are not fully captured.

While very few structural morphogenesis directly considers the seismic response of shell structures, the reasons have not been explicitly stated in literature. Nevertheless, the authors assume the reasons to be a combination of the following: (a) the conventional form-finding method (i.e. Thrust Network Analysis [11], Force Density Method [19] or Dynamic Relaxation Method [20]) is fundamentally a procedure in which a general (or conceptual) optimal geometry independent of the material is form-found in static equilibrium with dead load, and appropriate masonry blocks, reinforced concrete elements or gridshell members are subsequently assigned to the geometry. Hence, it is not easy to incorporate the cyclic response dependence of material and structural members in the first half of the method. (b) Furthermore, the computational cost of nonlinear response history analysis to evaluate the complex seismic response is huge compared with that of static analysis. Hence, it is not feasible and often unrealistic to adopt response history analysis directly for parametric designs of shell structures [15].

To overcome the computational problem mentioned in (b), Terazawa et al. [21–23] proposed a generalized response spectrum analysis (GRSA). GRSA is a series of numerical analyses which iteratively performs complex eigenvalue analysis and response spectrum analysis. GRSA quickly evaluates the seismic response of a 3D structural analysis model with finite viscous or elasto-plastic dampers, and thus is suitable for iterative (finite element analysis) FEA-based computational morphogenesis. The effectiveness of GRSA has been validated before in a size and layout optimization study [23,24] for seismic retrofit of a telecommunication tower in Japan using buckling-restrained braces, a large span music arena constructed in Japan [25], in a study investigating the seismic response characteristics of a damped outrigger system for tall buildings [26,27] and a novel damped braced tube system for a supertall building planed in Japan [28–30].

In this paper, GRSA-based computational morphogenesis of metal gridshell structures (with finite dampers) is proposed considering the response to both dead and seismic loads, and is then applied to metal gridshell roofs supported by buckling-restrained braced structures. The form-found structures are discussed in detail to evaluate the proposed method. In Section 2, an overview of the proposed method, the numerical simulation method to calculate objective functions, the definition of design variables and the constraints, and the adopted optimization algorithm are described in detail. A computational plugin having visual programming function for Grasshopper is also developed to accurately evaluate the computation time. In Section 3, the size and layout optimizations of buckling-restrained braces (BRBs) are carried out on the form-fixed spherical metal gridshell, and the obtained optimal BRB configurations for the computational morphogenesis of metal gridshell structures are discussed. In Section 4, the proposed method of simultaneously optimizing the roof shapes and BRB layouts in the substructures is applied to a three-story metal grid shell structure with a rectangular plan, and the effects of load combinations, seismic devices, given constraints to the form-found roof shapes and their dynamic response characteristics are discussed. In Section 5, the proposed method is validated and the conclusions are presented in Section 6. Note that this paper focuses on the effects of load types on the form-found roof shapes of specific building models and specific seismic intensity, and so the effects of epistemic uncertainties (such as those associated with the input ground motions and detailed numerical models) are outside the scope of the present study.

2. Computational morphogenesis considering the dead load and seismic response

2.1. Overview

The flowchart of the GRSA-based computational morphogenesis is shown in Fig. 1. In the proposed method, optimal damper layout and overall geometry for design are simultaneously searched for by the metaheuristic optimization algorithm (e.g. Genetic Algorithm and Particle Swarm Optimization) and finite element analysis (FEA) including GRSA. First, a population of design variables is randomly generated. Second, the objective functions of the design variables are evaluated by FEAs. Third, the design variables in the population are updated by the algorithm. Finally, the computation is terminated when the objective functions converge or the number of the generation (i.e. the iteration) reached the limitation. The analysis methods and the input ground motions are explained in Section 2.2. The design variable, the objective functions, and the constraints are explained in Section 2.3. The optimization algorithm is explained in Section 2.4. The practical computation environment on Rhinoceros + Grasshopper used in this paper is demonstrated in Section 2.5. The detailed definitions of the optimization problems are discussed in Section 3 and Section 4 later.

2.2. Analysis methods and input ground motions

The objective functions of the design variables are calculated by the conventional static analysis for dead load and the generalized response spectrum analysis [21–23] (GRSA) for a seismic load.

The flowchart of GRSA is shown in Fig. 2. GRSA is used to evaluate the equivalent modal characteristics and the seismic response of the structure considering the response modification by dampers.

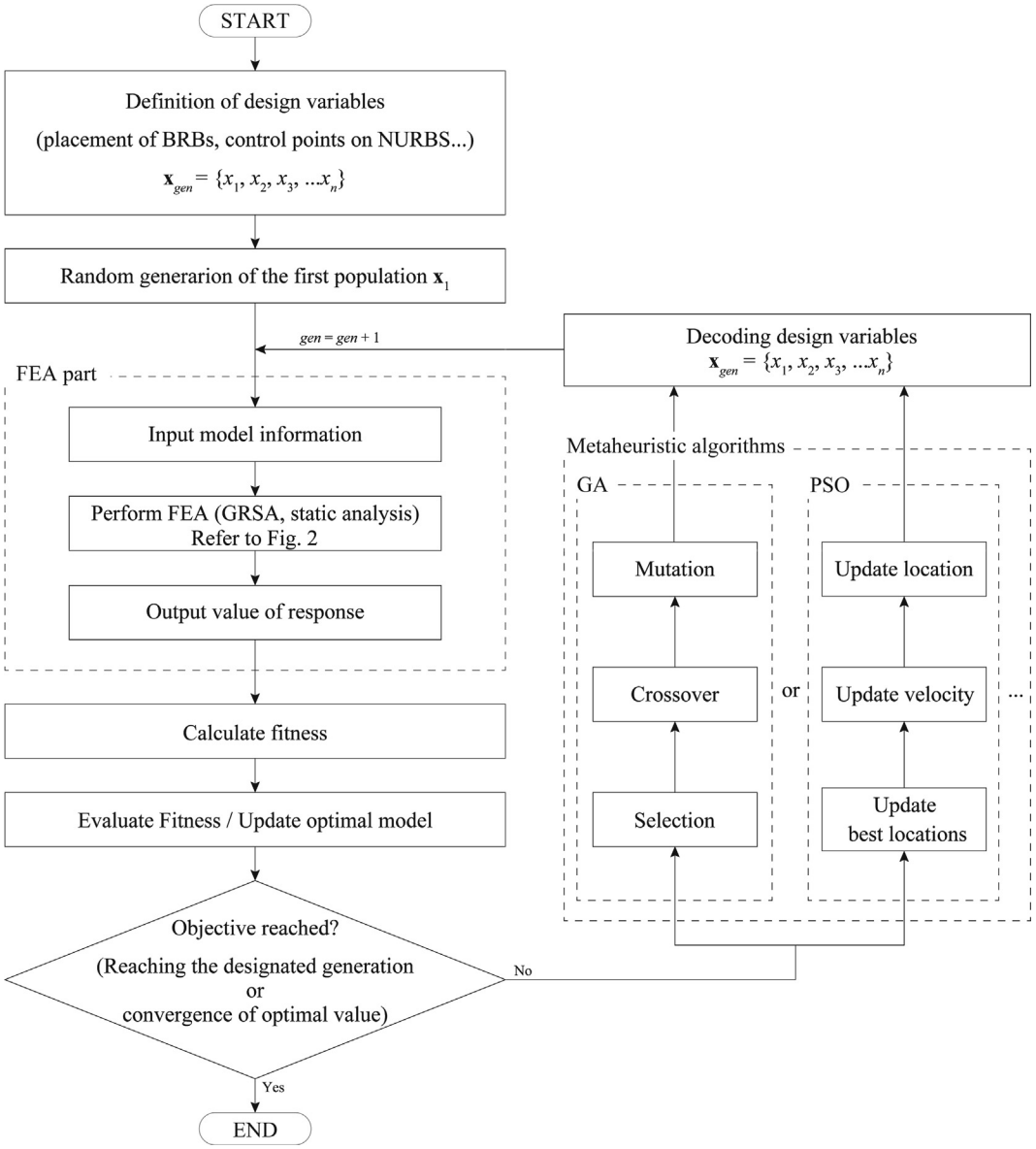

Fig. 1. Flowchart of GRSA-based computational morphogenesis.

GRSA is a series of numerical analyses iteratively conducting complex eigenvalue analysis and response spectrum analysis. The seismic response is evaluated from the complex eigenvalue of the substitute model with equivalent linearized elements simulating the nonlinearity of dampers, and a modified complete quadratic combination rule[31] for the non-proportional damping system as shown in Eq. (1).

$$R_{CQC} = \sqrt{\sum_{s=1}^{n}\sum_{r=1}^{n} B_s B_r S_s(\omega_s, \xi_s) S_r(\omega_r, \xi_r) \cos(\theta_s - \theta_r) \rho_{sr}} \tag{1}$$

Where n is the number of modes required to achieve modal mass participation of over 90 %, s and r are mode numbers, ξ is the modal damping ratio, ρ is the correlation coefficient of the various modes, ω is the natural circular frequency, S is the response spectrum value, $B = \mathrm{Re}(\lambda^* \beta\phi)/\sin(\theta)$,$\theta = \tan^{-1}(-\mathrm{Re}(\lambda^* \beta\varphi)/\mathrm{Re}(\beta\varphi))$, λ is the complex eigenvalue, β is the complex participation factor, φ is the complex eigenvector component, * is the complex conjugate.

In GRSA, the response spectrum values of the representative damping ratio (ξ_0 = 1, 2, 3, 5, 10, 15, 20, 30 %) are given beforehand from an external file, and the response spectrum value of the arbitrary damping ratio ξ, which is used in Eq. (1), are calculated by multiplying the response spectrum value of the closest ξ_0 with the response modification factor D_h[32] shown in Eq. (2).

$$D_h = \begin{cases} (\sqrt{(1+25\xi_0)/(1+25\xi)} - 1)(5T) + 1 & (0.0s \leqslant T < 0.2s) \\ \sqrt{(1+25\xi_0)/(1+25\xi)} & (0.2s \leqslant T < 2.0s) \\ \sqrt{(1+25\xi_0)/(1+25\xi)}\{\sqrt{\xi/\xi_0}(T-2)/40 + 1\} & (2.0s \leqslant T < 8.0s) \end{cases} \tag{2}$$

In the proposed method, only the material nonlinearities of dampers are considered and the main frame is designed to remain elastic. In this paper, a buckling-restrained brace e.g. [33–35] (BRB), which is a kind of hysteretic damper, is adopted in mid-rise supporting structures. In GRSA, the BRB is modeled as a link element with complex stiffness K_{eq} [21] where the axial stiffness is shown in Eq. (3). The material nonlinearity of BRB is modelled using the standard simple bilinear hysteresis rule composed of

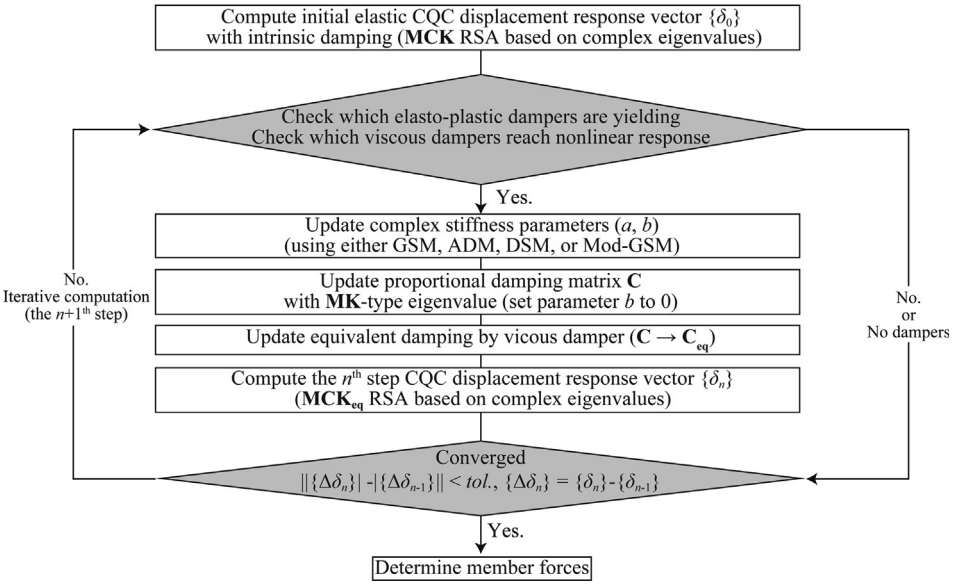

Fig. 2. Flowchart of GRSA [23].

the initial stiffness, yielding force, and post-yield stiffness ratio, considering kinematic hardening. The post-yield stiffness ratio is set to 2 % and the effect of cyclic hardening is included by introducing isotropic hardening by controlling the yield point. The corresponding parameters of complex stiffness adopted in GRSA are determined by these material parameters and the ductility factor of BRB. The complex parameters simulating the nonlinearity (i.e. the response reduction effect) of BRB are iteratively updated by the maximum response and the average damping method [21], as shown in Fig. 2. Note that a bilinear oil damper (where the damping force is proportional to the first power of the velocity) is also available in the current GRSA[23], but not adopted in this paper because viscous dampers are rarely used in mid-rise buildings.

$$K_{eq} = (a + ibsgn\omega_e)\frac{1}{L_p/L_0 + 2(L_e/L_0)(A_p/A_e)}\frac{EA_p}{L_0} \tag{3}$$

Where a is the equivalent stiffness parameter, b is the energy-dissipation parameter, i is the imaginary unit, sgn ω_e is the sign of the excitation circular frequency, L_0 is the length between the working points of the BRB, L_p is the length of the plastic yielding zone of the BRB, L_e is the length of the elastic zone of the BRB, A_p is the section area of the plastic yielding zone of the BRB, A_e is the section area of the elastic zone of the BRB, E is Young's modulus of steel material. In this paper, L_p/L_0 and A_p/A_e are assumed as 0.25 and 0.50, respectively.

Any seismic optimization model is always affected by epistemic uncertainties associated with the input ground motions, and previous research e.g. [36–39] on seismically isolated bridges have studied the effect of seismic intensity on the optimization result. Nevertheless, this paper focuses on the effect of load types (i.e. conventional dead load or dynamic seismic load) on the form-found roof shapes, and the epistemic uncertainties of seismic motion are outside the scope of the present study. In this paper, the site is assumed to be in Japan and accordingly, three Japanese spectrally matched seismic waves [40,41] (traditionally used in design practice) are assigned. The acceleration response spectra of the input ground motions and the design spectrum adopted from the Japanese design-base earthquake (DBE) level [40] are shown in Fig. 3. The Japanese DBE earthquake corresponds to a 473-year return period on the bedrock, and these ground motions are classified as non-frequent motions.

2.3. Design variables, objective functions, and constraints

The layout (as well as the size) of BRBs and the z-directional coordinates of the control points of the non-uniform rational b-spline (NURBS) (determining the overall geometry of the shell structure) are considered the design variables. The detailed definitions are described later in the design examples.

The main objective function to be minimized is defined in Eq. (4) subject to the given constraint. The mean peak seismic response against the design earthquake motions is the main objective function as expressed in Eq. (4), and a penalty is added if the seismic response of the structure does not satisfy the constraint.

$$F(x) = \frac{1}{n}\sum_{s=1}^{n}\max\{f_j(x,s)\,\big|\,j = 1,2,\ldots m\} + \phi \tag{4}$$

In Eq. (4), **x** is the design variable, n is the number of the design earthquake motions, **f** is the seismic response used as the objective function, m is the number of stories (the rotational angle) or 1 (the total strain energy of the roof members), and ϕ is the penalty function which equals 9999 (a large value) if the constraints are not satisfied. For example, in the proposed computational morphogenesis (Section 4), the z-coordinates of the control points of NURBS determining the geometry of the roof structure and the size of the BRB placed in the supporting structure are adopted as the design variables **x**. The total strain energy of roof members is adopted in the objective function **f**. The demand-to-capacity ratios (DCRs) of conventional braces in the supporting structure and the rotational angles (RAs) are adopted as the design constraints, and 9999 is assigned to the penalty function ϕ if the DCRs are over 1.0 or the RAs are over 1/100. The DCR and RA are described in the following paragraph.

In this paper, the rotational angle *RA* (Fig. 4), the total strain energy U of the roof members, and the demand-to-capacity ratio DCR of the member buckling are assigned as the objective function or as constraints. *RA* is calculated using the relative displacement of the nodes of the members (Eq.(5)) and acts as a simple unified index of both the story drift angle and the member rotation angle. In practice, the design criteria for *RA* is defined using the performance limit based on the damage tolerances of the structure and the dropout limit of the finishing material. In this study, *RA* is assigned as both the objective function and the constraint where *RA* is limited to 1/100, a typical value in Japan.

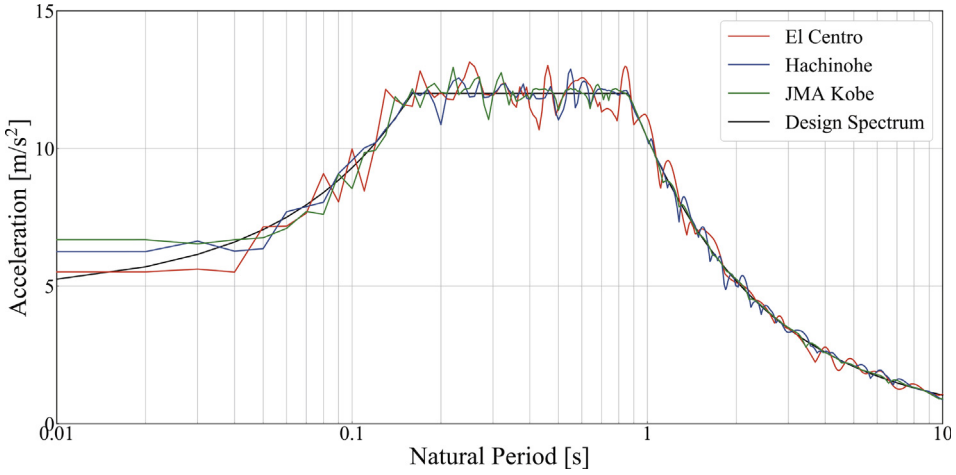

Fig. 3. Acceleration response spectra of input ground motions (ξ_0 = 5 %).

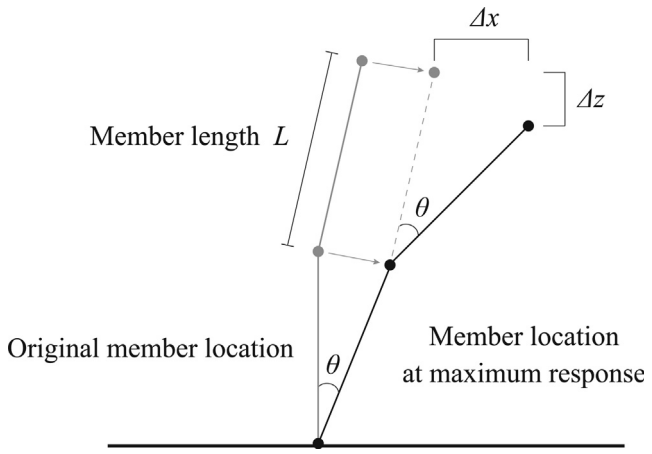

Fig. 4. Definition of rotation angle *RA*.

$$RA \approx \tan\theta = \frac{\sqrt{\Delta x^2 + \Delta z^2}}{L} \tag{5}$$

The total strain energy (also called "compliance") of the roof member U is calculated following Eq. (6). In a conventional shape optimization under static loads (i.e. dead loads), U is typically assigned as the objective function to maximize the static stiffness of the structure. Following this tradition, in Section 4, the effect of the load combination and the design constraint to the optimal geometry, where the dynamic stiffness is maximized, is discussed. Note that in the load combination considering bi-directional seismic inputs, U in each direction is multiplied by $2^{0.5}$, and is summed as U of 45-degree directional input.

$$U = \frac{1}{2}\sum_{k=1}^{MEM}\frac{A_k L_k}{E_k}\left({}_k\sigma_N^2 + k(2)\sigma_M^2 + k(2)\sigma_M^2\right) \tag{6}$$

where MEM is the number of the members, A_k is the section area, L_k is the member length, E_k is Young's modulus, ${}_k\sigma_N$ is the nominal axial stress, ${}^{(i)}{}_k\sigma_M$ is the nominal bending stress of i-end of the member.

In the calculation of the buckling demand-to-capacity ratio (DCR) for each member, the capacity is computed following the AIJ standard [42]. Since buckling causes a significant reduction of the stiffness leading to large (unacceptable) deformations[6,7], DCR considering buckling is assigned as the constraint in this paper.

2.4. Optimization algorithm

The dynamic response characteristics of gridshells are significantly influenced by the member configuration and the shell geometry, and so to perform seismic optimization e.g. [22,24,25,28], the gradient-based optimization algorithm is not necessarily feasible. Moreover, this algorithm is computationally expensive because of the large number of the degree-of-freedoms in the 3d models. Therefore, in this paper, the metaheuristic method (i.e. the commonly used Particle Swarm Optimization (PSO)) is adopted in the proposed computational morphogenesis. The parameters used for the optimization algorithms are summarized in Table 1. The size of the population is set as 30. In Section 3 and Section 4, convergence was confirmed by repeating the optimizations at least twice. Note that the optimization algorithm was run for 50 generations and termination-based convergence of the objective function is outside the scope of this paper.

2.5. Computing environment

A plugin having visual programming function was developed for Rhinoceros + Grasshopper[3] (a 3DCAD software) to accurately evaluate the computation time (including the time loss by the data linkage between 3DCAD and external software). The computational workflow is shown in Fig. 5. A numerical simulation framework [21] previously coded by the first author using Fortran 90/95 was adopted to develop the plugin. The plugin was coded in C# and is hereafter called "Titan" (after the nickname of the school emblem of Tokyo Institute of Technology). As shown in Fig. 5, the workflow can be summarized as follows:

(1) Randomly generate the initial design variables (in Titan).
(2) Construct the 3DCAD model (in Rhinoceros + Grasshopper).
(3) Export the 3DCAD model data as a text file to use as input for the numerical model (in Titan).
(4) Perform FEAs (in Titan).
(5) Calculate the objective functions from the FEA results (in Titan) and.
(6) Update the design variables by the optimization algorithm (in Titan).

Table 1
Specifications of optimization algorithms.

Particle Swarm Optimization (PSO)		
Inertia w	Personal best weight c_1	Global best weigh c_2
1.0	2.0	2.0

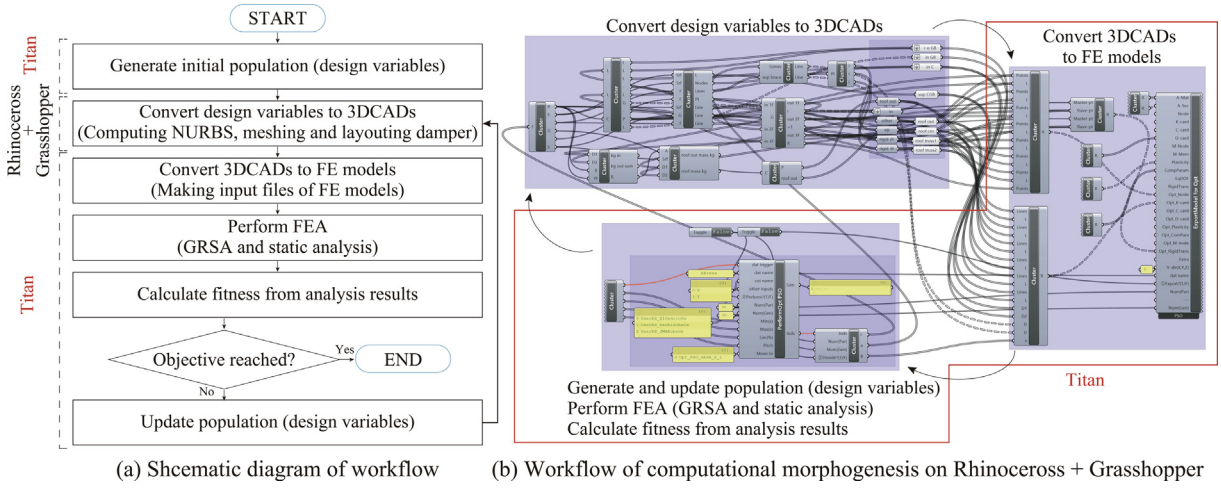

Fig. 5. Workflow with Rhinoceros + Grasshopper.

The whole computational workflow was run on a local workstation equipped with the Intel Core i9-7940X (14 processors with 3.10 GHz) and a 64 GB DDR4-RAM. For this study, 14 FEAs were run in parallel and one processor was assigned for each FEA.

3. Optimal BRB layout in metal spatial structures

Past researchers e.g. [43] working on passive response control of gridshell structures placed dampers not only in the supporting structures but also in the roof. Hence, in this section, a series of layout optimization of BRBs is carried out on the spherical metal gridshells keeping the roof geometry fixed, and an appropriate BRB layout is then discussed for computational morphogenesis.

3.1. Target structures

The target structure as shown in Fig. 6(a) is a spherical metal gridshell structure like a geodesic dome. The lower floors are assumed to be for retail stores and MEP (mechanical, electrical, and plumbing), and the upper floors are assumed to be assigned for events. The perimeter gridshells work as both the perimeter walls and roofs. The geometry of the entire structure is controlled by two parameters - the base diameter D and the maximum height H. Three different configurations are considered as shown in Fig. 6 (b). The layout optimization of BRBs was carried out on the substructure of the three structures to investigate the relationships between the optimal BRB layout and the overall geometry. The "H30-D60" model is a domed roof and has a two-story substructure, the "H60-D30" configuration resembles a taller multistory building with a curved roof, and the "H45-D45" model has a configuration in between the other two.

The member specifications are listed in Table 2. A roof and wall dead load of 1.2 kN/m^2, and a floor dead load of 5 kN/m^2 was assumed. The members were designed for a load combination of the dead loads and the horizontal equivalent static seismic loads using a peak ground acceleration of 0.2 g (Japanese service-level earthquake) according to the allowable strength design based on the design standard [42] of the Architecture Institute of Japan

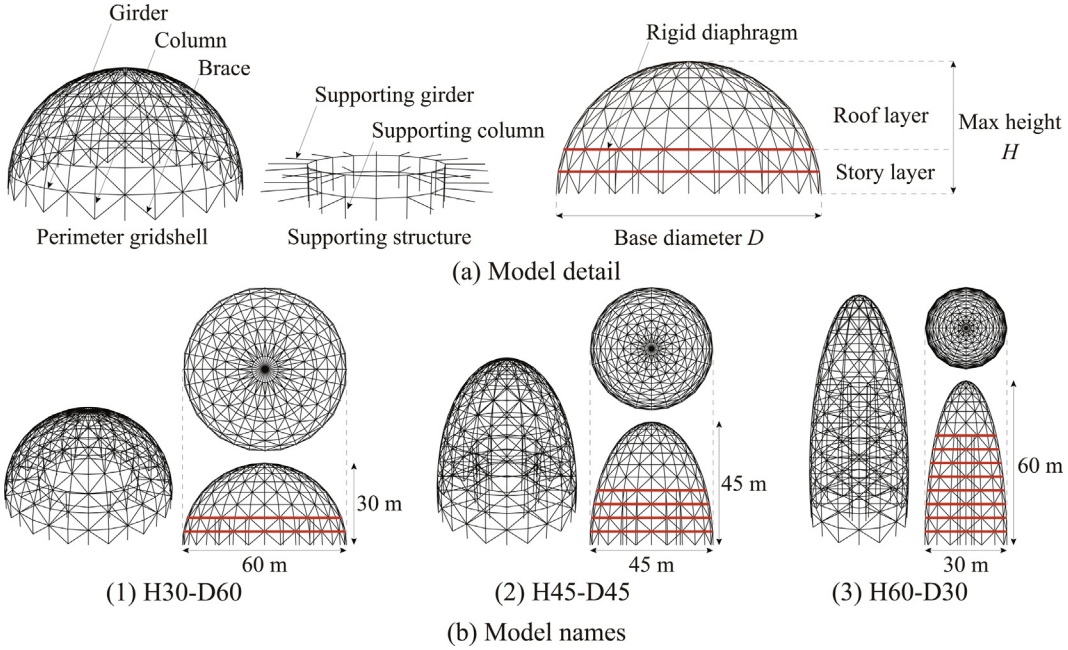

Fig. 6. Numerical models of the target structures.

Table 2
Member specification.

Member		H30-D60	H45-D45	H60-D30
Roof layer	Column Girder Brace	φ318.5 × 12.7	φ355.6 × 12.7	φ406.4 × 12.7
Story layer	Column	φ318.5 × 12.7	φ457.4 × 19.0	φ508.0 × 19.0
	Girder	φ318.5 × 12.7	φ355.6 × 12.7	φ406.4 × 12.7
	Brace			
	Supporting column	H-700 × 300 × 12 × 25		
	Supporting girder	φ609.6 × 22		

(AIJ). The height of each story layer is fixed at 5 m. The number of floors is three for H30-D60, five for H45-D45, and nine for H60-D60, respectively. In the numerical models, the members were modeled as elastic beam elements, and rigid diaphragms were assigned to the floors. The column ends of the perimeter gridshell are fixed supports, and those of the supporting structures are pinned supports. Rayleigh-type proportional damping matrix composed of the initial stiffness and initial mass matrix is adopted, setting the first and second predominant mode's initial damping ratios to 2 %. Unidirectional seismic inputs are adopted considering the symmetry of the target structure.

The modal characteristics of the initial (pre-optimized) models are shown in Fig. 7(a). In H30-D60, the complex coupled horizontal-vertical vibration modes typically observed in curved spatial structures were predominant. In H60-D30, the horizontal sway modes typical to multi-story buildings were predominant. In H45-D45, intermediate (vertical and horizontal) vibration modes were predominant. The RA responses of the ridgeline members of the perimeter gridshell and the member DCR responses are shown in Fig. 7(b). In all the models, the peak RAs were lower than 1/150 rad. (an acceptable story drift ratio), but the DCRs in the relatively heavy story layers are over 1.0. The seismic performance of the initial models was thus not satisfactory enough against the DBE level earthquakes.

3.2. Definition of optimization problems

A schematic diagram depicting the design variables is shown in Fig. 8 and summaries of the PSO-based layout optimization of BRBs (with the variable as the BRB size) are given in Table 3. In the optimization process, the diagonal braces on the perimeter gridshell are replaced with BRBs. The BRB size is chosen from a fixed range consisting of 0kN (meaning no replacement of the braces), 500kN, 1000kN, and 1500kN. As shown in Fig. 8, the design variable is the chosen BRB size (per BRB). The dimension of the design variable is the number of stories (=8 in this case). The main objective is the RA demand, and the constraint is that the DCRs should be lower than 1.0 (implying no member buckling occurs). The objective function considering the constraint is calculated by Eq.(4) as per Section 2.3.

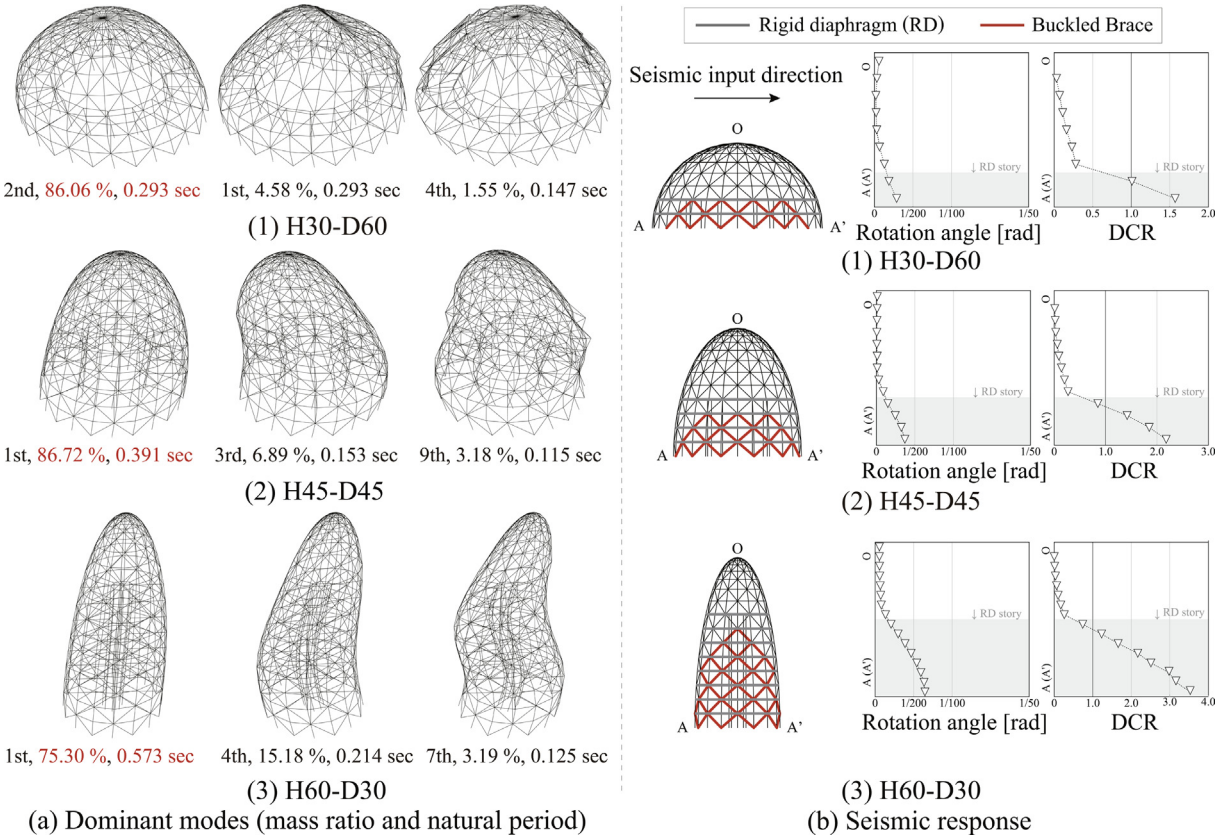

Fig. 7. Dynamic response characteristics of initial models (with no BRB).

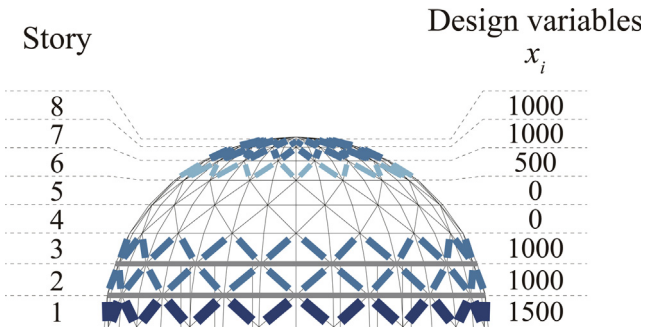

Fig. 8. Schematic diagram of design variables.

Table 3
Summary of the optimization problem.

Model	H30-D60	H45-D45	H60-D30
Optimize	BRB layout (Variable = BRB size)		
Variables	x_i = 0 kN (no replacement), 500 kN, 1000 kN, 1500 kN		
Minimize	Rotation angle (RA)		
Subject to	DCR < 1.0		
Algorithm	Particle swarm optimization (PSO)		
Number of variables	8	12	15

3.3. Layout optimization results considering variable BRB size

The optimal BRB layouts and the corresponding seismic responses are shown in Fig. 9, where T_{eq} and ξ_{eq} are the equivalent first mode secant period, and the equivalent first mode damping ratio, respectively, considering the nonlinearity of BRBs. During the optimization, the braces in the story with a DCR of over 1.0 in the initial model tended to be replaced with BRBs to prevent member buckling. Regardless of the overall geometry, larger BRBs were placed towards the lower stories, which is similar to a typical optimal damper distribution [32] in multi-story buildings. In all the optimized models, the DCRs in the upper stories on the story where the braces were replaced with BRBs significantly reduced to <1.0. This result indicates that the BRB acts as a seismic fuse (due to the force-limiting effect [24]) and can effectively control the seismic input to the roof or superstructure. Alternatively. BRBs may be placed on the roof layer, but as these do not yield, they contribute to only the stiffness of the roof layer by functioning as elastic braces. In addition, RAs for all models were confirmed to be<1/200 rad., the beams and columns remained elastic with no damage, and the dropout of the finishing material was also prevented.

3.4. Discussion

During the optimization, BRBs were actively placed in the heavier story layer rather than the roof layer. If BRBs are placed in the roof layer, they only contribute to the stiffness of the roof and do not provide any (seismic) energy dissipation. An increase in the number of stories increases the building weight, which increases the number of required BRBs as observed in the optimization results. Nevertheless, variation in structural geometry (for example, a larger D/H ratio behaving as a spherical roof with a low-rise substructure or a smaller D/H ratio behaving as a taller multi-story-building with a curved roof) was found to have no significant effect on the optimal layouts of BRBs in gridshells with relatively heavy lower stories (i.e. the supporting structure). Therefore, for computational morphogenesis discussed in the next section, the BRBs (i.e. dampers) were placed in the supporting structure.

4. Computational morphogenesis of metal grid shell roofs with supporting structures

In Section 4, computational morphogenesis is performed on metal gridshell roofs with supporting structures, and the effects of the load combination, the response reduction by BRBs, and the constraints on both the geometry of the roof structure and the dynamic response characteristics are investigated.

4.1. Target buildings

The target building shown in Fig. 10 is a three-story metal grid shell structure with a rectangular plan (36 m × 60 m) and is assumed to represent a typical sports facility.

The frame member specifications are listed in Table 4. A roof and wall dead load of 1.2 kN/m^2, and a floor load of 5 kN/m^2 are assumed. The initial (before optimization) buildings are designed using Japanese conventional braced frames (CBF) against a combination of the dead load and a horizontal equivalent static seismic load considering a peak ground acceleration of 0.2 g as per the allowable strength design in the design standard [42] of the Archi-

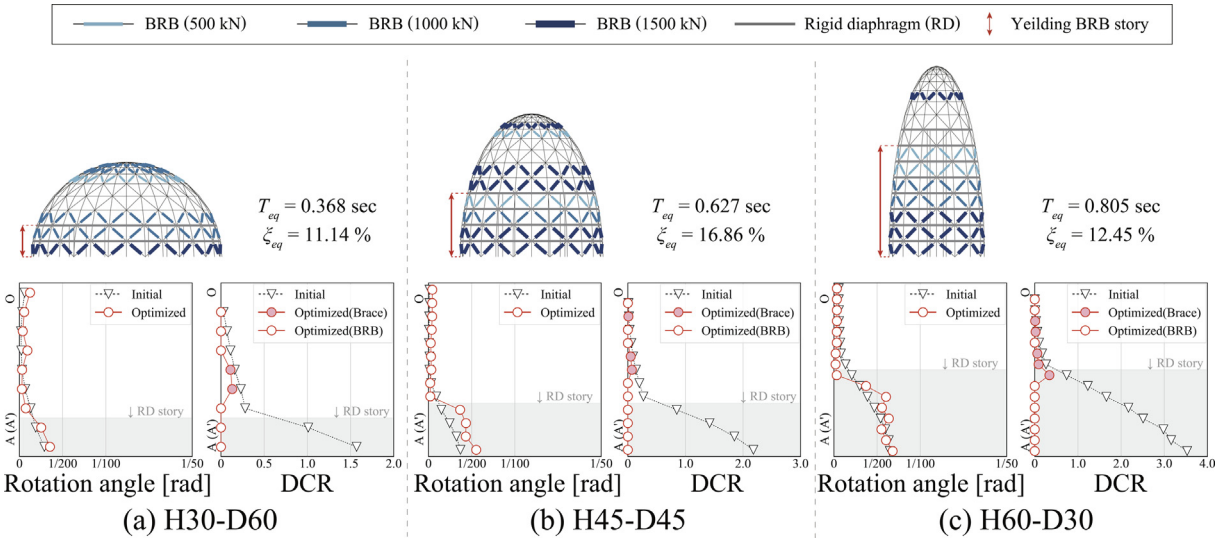

Fig. 9. Optimization results.

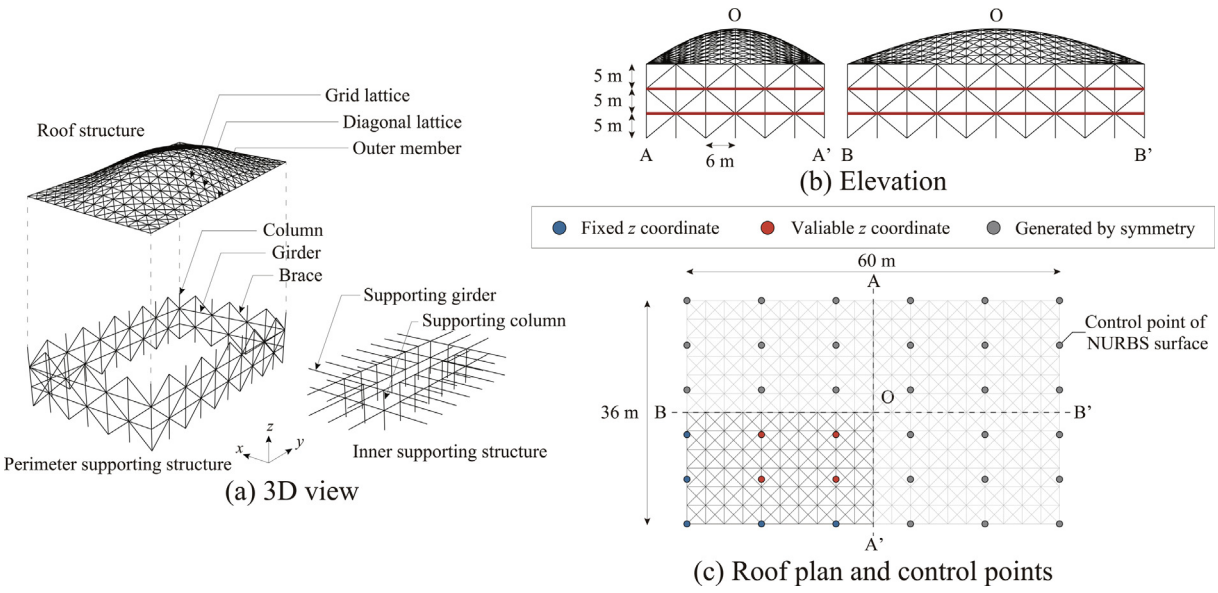

Fig. 10. Numerical models of target structures.

Table 4
Member specification.

Member		Section
Roof structure	Grid lattice	φ355.6 × 12.7
	Diagonal lattice	φ26
	Outer member	φ457.2 × 19
Perimeter supporting structure	Column & Girder	φ457.2 × 19
	Brace	φ216.3 × 8.2
Inner supporting structure	Supporting column	H-700 × 300 × 12 × 25
	Supporting girder	φ609.6 × 22

tecture Institute of Japan (AIJ). The nodal coordinates and member locations of the roof structure are determined by projecting the planar grid shown in Fig. 10 on the 3D surfaces. The geometry of the roof structure is based on the NURBS surface. The initial shapes of the roof structures are designed so that the roofs have a moderate rise similar to that of a shallow shell. As shown in Fig. 10, based on the symmetry of the plan, the number of control points of the NURBS is four for the rectangular plan model.

In the numerical models, the diagonal lattice in the roof structure is modeled as an elastic truss element, and the other members are modeled as elastic beam elements. A rigid diaphragm is assigned to the floors of the supporting structures. The column ends of the supporting structures are pinned supports. Rayleigh-type proportional damping matrix composed of the initial stiffness and initial mass matrix is adopted, and the first and second predominant mode's initial damping ratios are set to 2 %.

The dominant modes of the initial models are shown in Fig. 11 (a). Coupled vibration modes consisting of the horizontal sway mode of the supporting structure and the horizontal-vertical vibra-

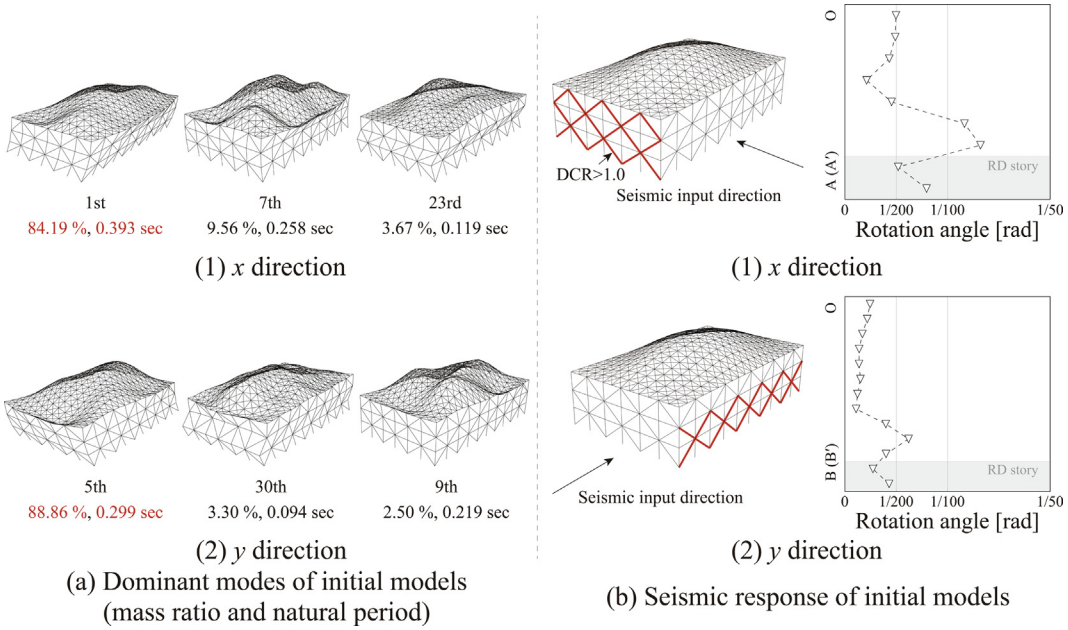

Fig. 11. Dynamic response characteristics of Initial models.

tion mode of the roof structure are predominant. The RA responses of the ridgeline members are shown in Fig. 11(b). Members with a DCR of over 1.0 are indicated in red on the axonometric drawing. In all models, the *x*-directional RAs are larger than the *y*-directional RAs. Similarly, the *x*-directional RAs in the roof structure are over 1/100 rad. indicating that the finishing material has dropped out. The RAs in the supporting structure are<1/100 rad. (an acceptable value described in Section 2.3), but the corresponding DCRs are over 1.0.

4.2. Definition of the optimization problem

The definitions of the optimization problems and the corresponding model IDs are given in Table 5. The optimization problems are subdivided based on the type of seismic devices, the load combination, and the constraints. Two seismic energy dissipation devices- a conventional brace (CB) or a BRB are allowed. The adopted load combinations are as follows: (1) the dead load and an *x*-directional seismic load (DL + ELx), (2) the dead load and a *y*-directional seismic load (DL + ELy), and (3) the dead load and a bi-directional seismic load (DL + ELxy). The constraint is that the member DCRs should be<1.0 (meaning no buckling) or the RAs should be<1/100 rad. (meaning no damage to the mainframe). As a result, 10 optimal overall geometries of the metal gridshell roofs are found. R-CB-DL is the conventional form-found shape considering only the dead load. The R-CB-DLEL series are form-found shapes considering both the dead load and the seismic response. Furthermore, the R-BRB-DLEL series are the form-found shapes also considering the response reduction effect by BRBs (i.e. dampers) and the R-BRB-DLEL-RA series models are form-found considering the response reduction effect by BRBs and the drift limit. The schematic diagram depicting the design variables is shown in Fig. 12. For the R-CB- series, the design variables are the *z*-coordinates of the control points of NURBS determining the geometry of the roof structure. The design variables for the R-BRB- series also include the size of the BRB placed in each story. Note that in practical computational morphogenesis[1] for design, the *z*-coordinates of the control points of the geometry may be strictly constrained by the initial shape predetermined by the architect. Nevertheless, in this study, for investigating the efficiency of the proposed method, the optimal geometry following structural rationality is searched for and additional architectural design constraints are ignored. So, the main objective function is the total strain energy demand of the roof members.

4.3. Form-finding results

4.3.1. Form-found roof shapes and modal characteristics

The axonometric drawing and the ridgeline shapes are shown in Fig. 13(a), and Fig. 13(b), respectively. The modal characteristics of the form-found models are shown in Fig. 14.

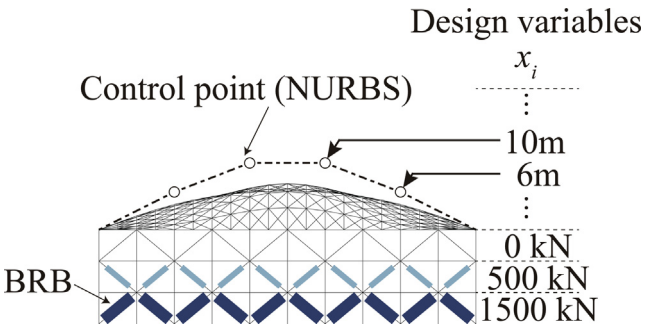

Fig. 12. Schematic diagram depicting an example of the design variables.

The R-CB-DL model found only considering the dead load is a traditional funicular compression roof shape with high static stiffness, and its rise (along the ridgeline) is the highest among all the form-found geometries. In contrast, for the R-CB-DLEL series found considering the dead load and the dynamic seismic loads, a relatively flattened but locally bulged roof shape is found. Their rises (along the ridgeline) are significantly lower than the other series (about 20 % of that of R-CB-DL). As shown in Fig. 14, particularly in R-CB-DLELx and R-CB-DLELxy, the horizontal sway modes (where the roof behaves like a rigid body) are predominant in the *x*-direction. Compared to the initial models, the dominance of the horizontal-vertical vibration mode of the roof structure shown in Fig. 11(a) is mitigated. These shapes effectively minimize the total strain energy of the roof members under seismic load, and this result suggests that a relatively flattened shape is more efficient in providing high dynamic stiffness. Similar shapes were found in a previous shape optimization study[17] maximizing the linear buckling load of a single-layer latticed shell structure using equivalent static seismic loads. Hence, this general conclusion may be universally applicable.

For the R-BRB-DLEL models form-found considering the response reduction effect by BRBs, the rise (along the ridgeline) is between those observed in the R-CB-DL and the R-CB-DLEL models. This result indicates that the optimal geometry under seismic loads is close to a funicular structure when the dampers effectively reduce the seismic input to the roof structure and the ratio of the total strain energy against the dead load case is higher (as shown in Fig. 15). Note that the equivalent natural periods are longer if compared to the initial models, and the obtained equivalent damping ratios are significantly larger than the initial damping ratios (2 %) as shown in Fig. 16.

For the R-BRB-DLEL-RA models form-found considering the response reduction effect by BRBs and the drift limit, the rises (along the ridgeline) are lower than those of the R-BRR-DLEL series (form-found not considering the drift limit), but are close to those of the R-CB-DLEL models (form-found not considering the response reduction effect). The equivalent natural periods of the R-BRB-

Table 5
Optimization problems and model IDs.

Model ID	R-CB-DL	R-CB-DLELx, R-CB-DLELy, R-CB-DLELxy	R-BRB-DLELx, R-BRB-DLELy, R-BRB-DLELxy	R-BRB-DLELx-RA, R-BRB-DLELy-RA, R-BRB-DLELxy-RA
Seismic device	CB	CB	CB & BRB	CB & BRB
Load	DL	DL + ELx, DL + ELy, DL + ELx + ELy	DL + ELx, DL + ELy, DL + ELx + ELy	DL + ELx, DL + ELy, DL + ELx + ELy
Type				
Subject to	N/A		DCR < 1.0	DCR < 1.0 & RA < 1/100 rad.
Optimize	Roof shape		Roof shape & BRB layout	
Variables	$0 \le x_i \le 20$ m, $0 \le i \le 3$		$0 \le x_i \le 20$ m, $0 \le i \le 3$ $0 \le x_i \le 1500$ kN, $4 \le i \le 6$	
Minimize	The total strain energy of roof members			
Algorithm	Particle Swarm Optimization (PSO)			

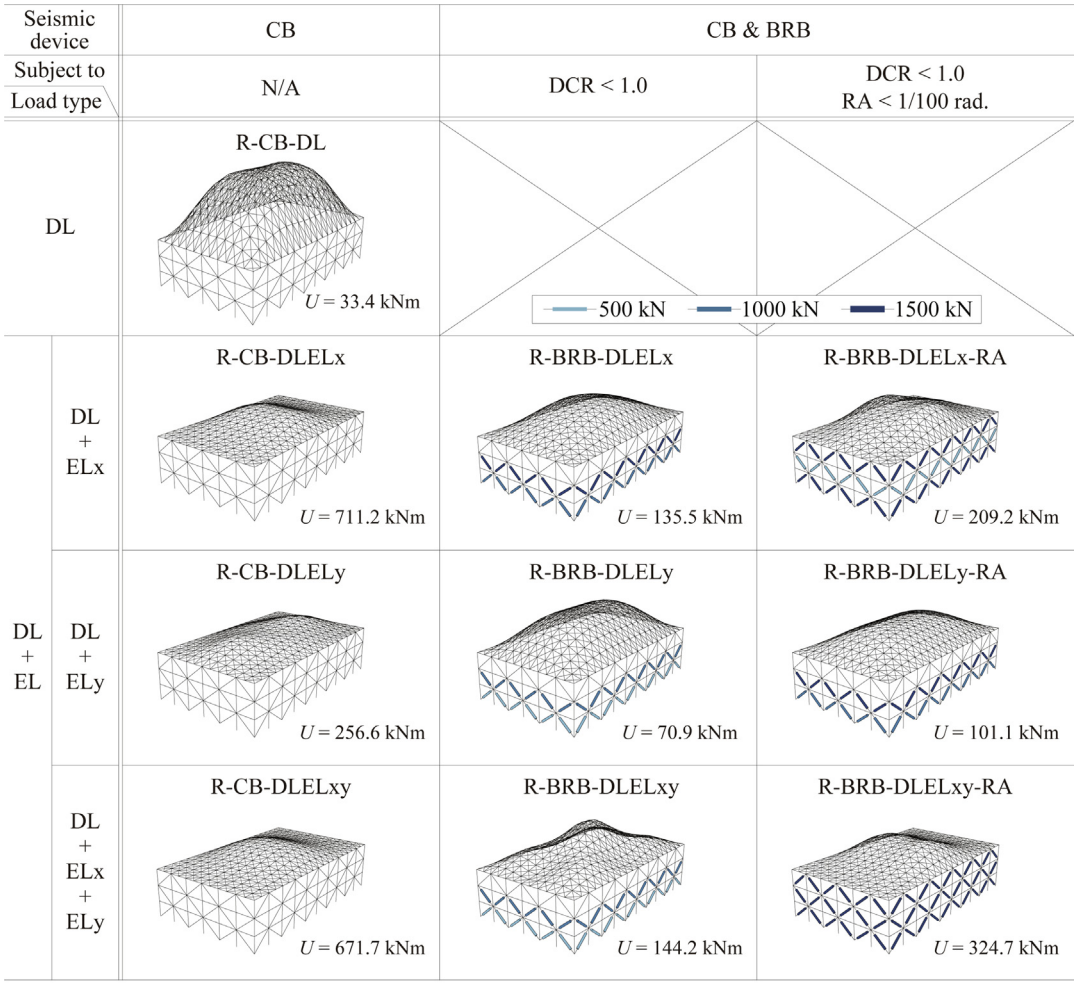

(a) Form-found models

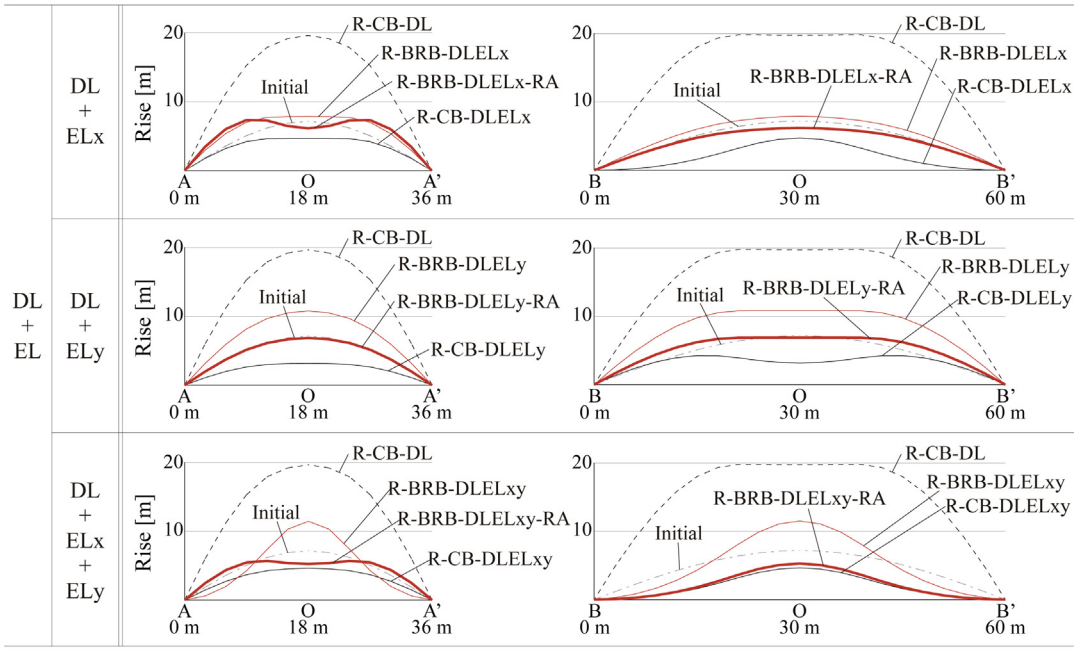

(b) Ridge line of form-found models

Fig. 13. Geometry of form-found structures (rectangular plan model).

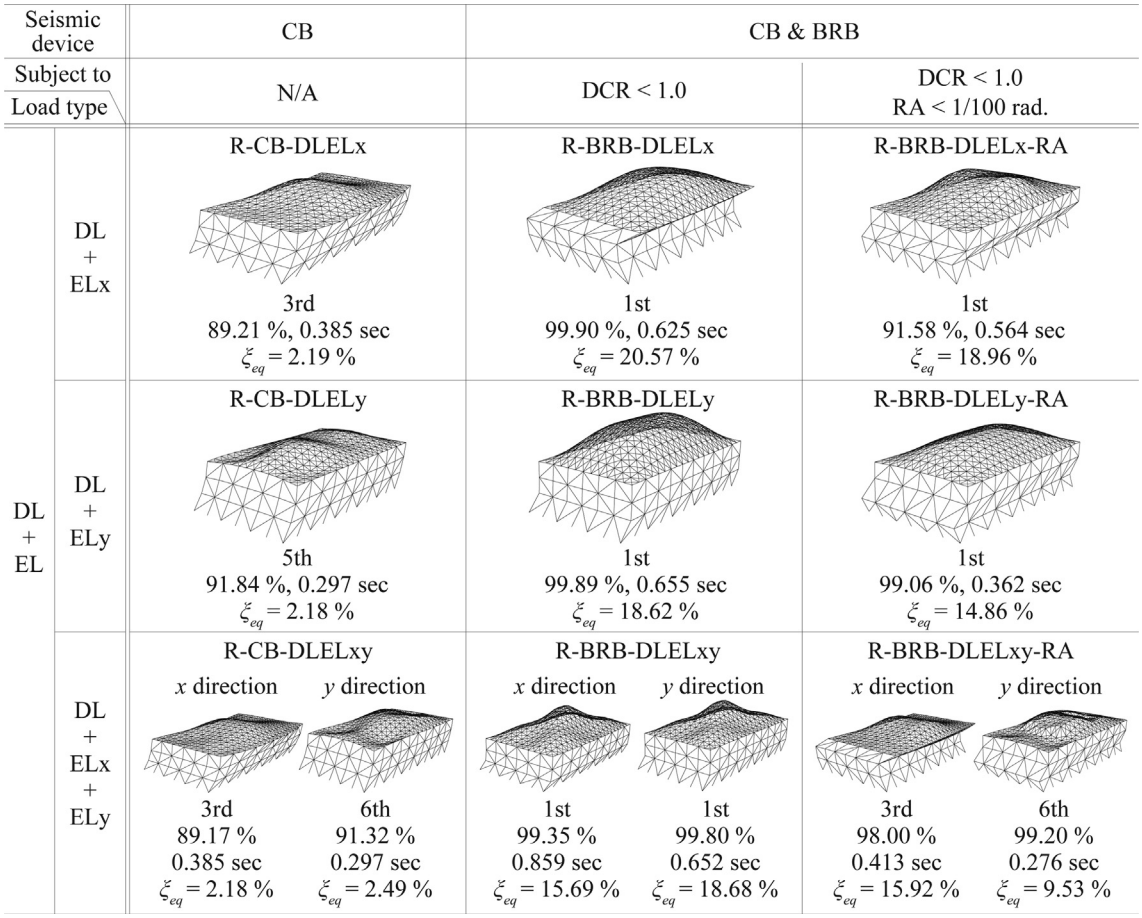

Fig. 14. Dominant modes of form-found models.

DLEL-RA series are shorter than those of the R-BRB-DLEL series, and are closer to those of the R-CB-DLEL models. Therefore, the form-found roof shapes may be affected by this period elongation that is dependent on the seismic input.

As shown in Fig. 13, the form-found roof shapes were found to be significantly influenced by the load combinations, and therefore a generalized optimal geometry (often focused on in the past form-finding-based research) was not obtained even for a simple regular rectangular plan.

4.3.2. Static and dynamic response of form-found structures

The RA responses and the total strain energy of the form-found models are shown in Fig. 15. The axial forces and bending moments of the members are shown in Fig. 16. In Fig. 16, only the R-CB DL and R-BRB-DLEL series are shown for brevity.

The total strain energy of the form-found roof shape considering only the dead load (R-CB-DL) is the lowest among all the models. The corresponding axial forces and bending moments are also lower than those in the other shapes. However, its RA responses under seismic loads are over 1/100 rad, and the corresponding axial forces and bending moments are significantly larger than those of the form-found roof shapes considering the seismic response. This result indicates that the conventional structural morphogenesis considering only the dead load does not guarantee structural safety against extreme seismic loads.

In contrast, for the R-CB-DLEL series and R-BRB-DLEL series (form-found considering both the dead load and the seismic loads), the member forces of the form-found roofs against the dead load are larger than those of the R-CB-DL models, and the corresponding responses are significantly smaller if compared against the seismic loads. For the R-BRB-DLEL series and R-BRB-DLEL-RA series (obtained considering the response reduction effect by BRBs), the corresponding member forces under the seismic load are further reduced from those of the R-CB-DLEL series and R-BRB-DLEL series. As shown in Fig. 16, the R-BRB-DLEL-RA series (form-found considering both the response reduction effect by BRBs and the drift limits) prevent damage to the supporting structure. Consequently, the reduction effect by BRBs (to the seismic input to the roof structure) decreases, and the total strain energy of the roof members is larger if compared to the energy of the R-BRB-DLEL.

4.4. Buckling load capacity of the form-found metal gridshell roof

The buckling load capacities of the members (not considered for the computational morphogenesis) of the form-found roofs are verified in this section. The linear buckling load factors obtained from buckling analysis are summarized in Table 6. Following the design example in the design recommendation [44] of the International Association for Shell and Spatial Structures (IASS), the elasto-plastic buckling load factors may be assumed as 0.2 (including a reduction ratio of 0.5 from shape-based initial imperfection and a reduction ratio of 0.4 from member yielding) times the linear buckling load factors. The roof shapes with a high rise (R-CB-DL) have high static stiffness and are less prone to global buckling than the others. Nevertheless, even the flattened roof shapes which are resilient against the seismic responses have elasto-plastic buckling load factors in the range of 4.58 (R-BRB-DLELxy-RA) to 11.10 (S-BRB-DLELy), and thus these form-found roof shapes considering both the dead load and the seismic load have enough safety margin to prevent global buckling.

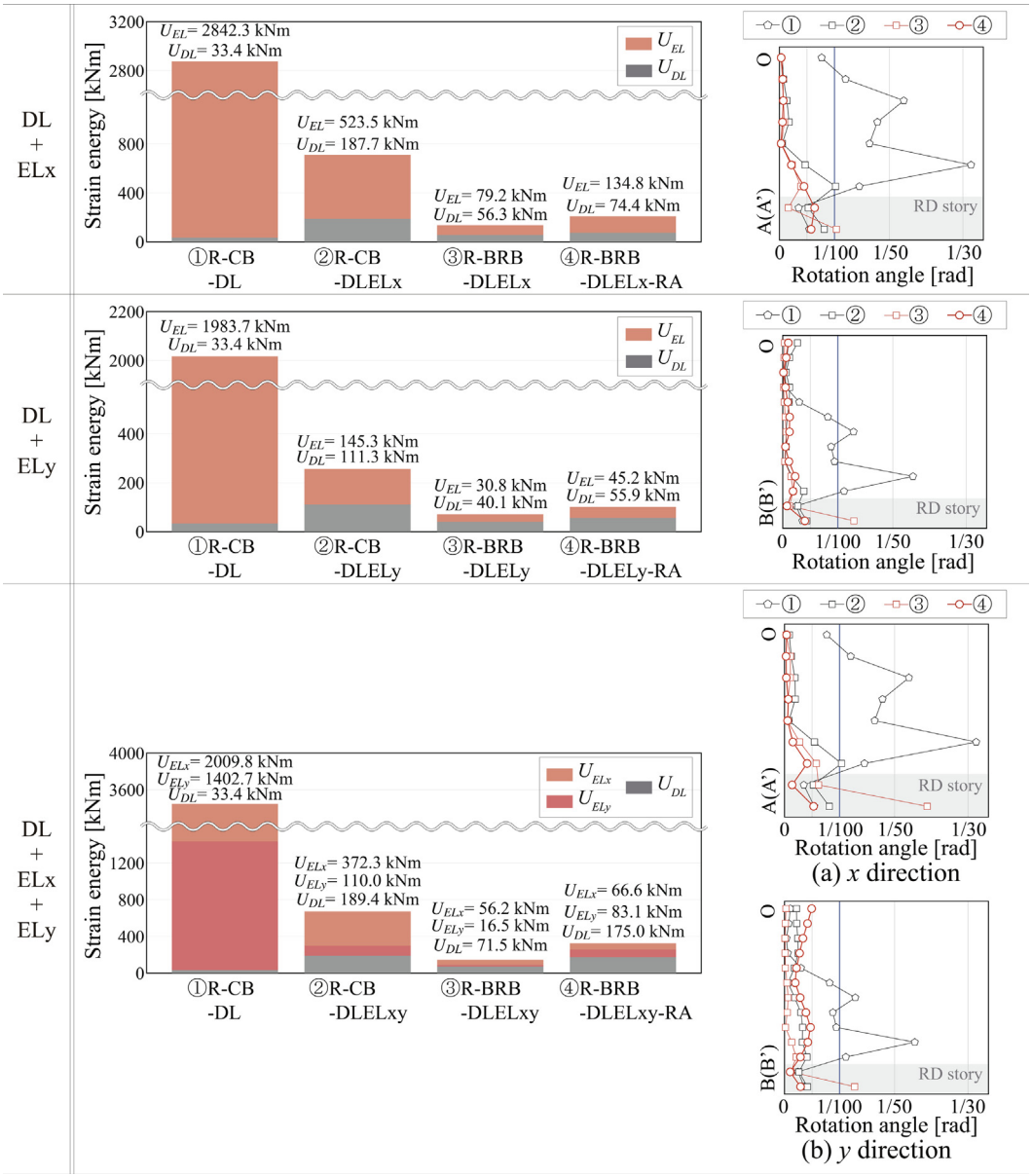

Fig. 15. Seismic response and strain energy (GRSA and static analysis).

5. Evaluation of GRSA-based computational morphogenesis

5.1. Accuracy of GRSA

Responses from GRSA and NLRHA on the form-found models of R-BRB-DLELxy are compared in Fig. 17. The seismic responses of the initial models and the form-found models under only the dead load are also shown in the figures. The Newmark β numerical method was adopted for the NLRHA to calculate the incremental displacement. While GRSAs evaluated the deformation-controlled responses (like the RAs) with sufficient practical accuracy, the vertical acceleration responses might be underestimated by up to about 0.8 g, particularly in the models defined in Section 3. This is because GRSA evaluates the seismic response based on equivalent modal characteristics of the substitute model adjusted to an assumed peak displacement response, but the peak acceleration may occur at a different time than the peak displacement. In other words, the modal characteristics when the maximum acceleration response occurs may be different from those used in the GRSA. Nevertheless, the acceleration responses of most of the form-found models were smaller than those of the initial models, which suggests that the proposed method finds a roof shape that is efficient even at reducing the acceleration response. Therefore, despite this minor error (left up to a user's judgment), it is recommended to use the proposed GRSA-based computational morphogenesis for the parametric studies and perform NLRHA only as a final design check.

5.2. Computation time

The computation times are listed in Table 7. The computation time of a single GRSA is significantly less than that of a single NLRHA which took 20 to 30 min for the models in this paper. The total computation time was about 15 h for the workflow considering the load combination of the dead load and uni-directional seismic load, and 27 h for the load combination considering the bi-directional seismic load due to the negligible effect of the number of seismic waves and iterations (i.e. generations of the optimization algorithm). These time durations may be further reduced as follows: (a) evaluate the seismic response using only the design

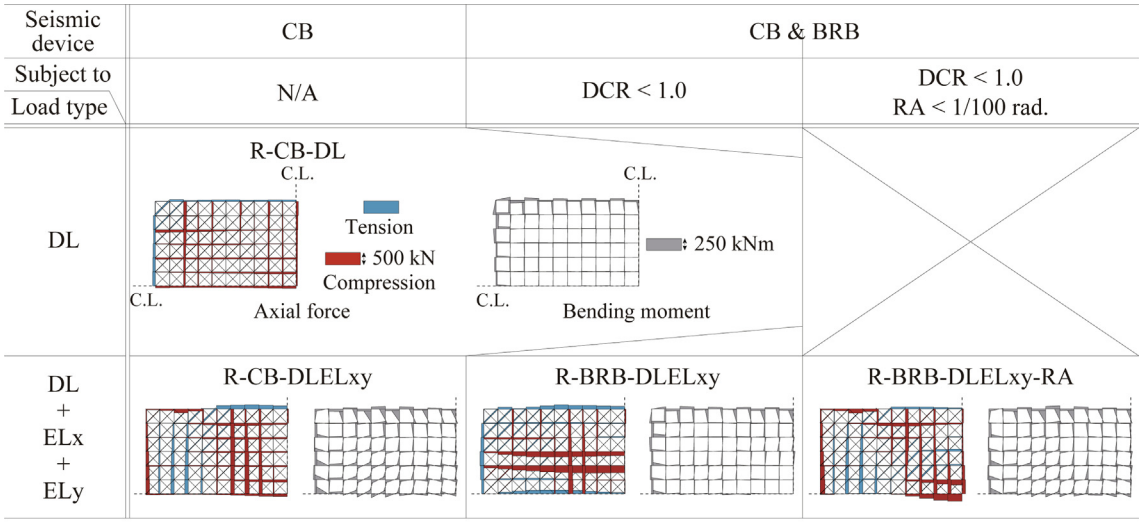

(a) Member force distribution by dead load

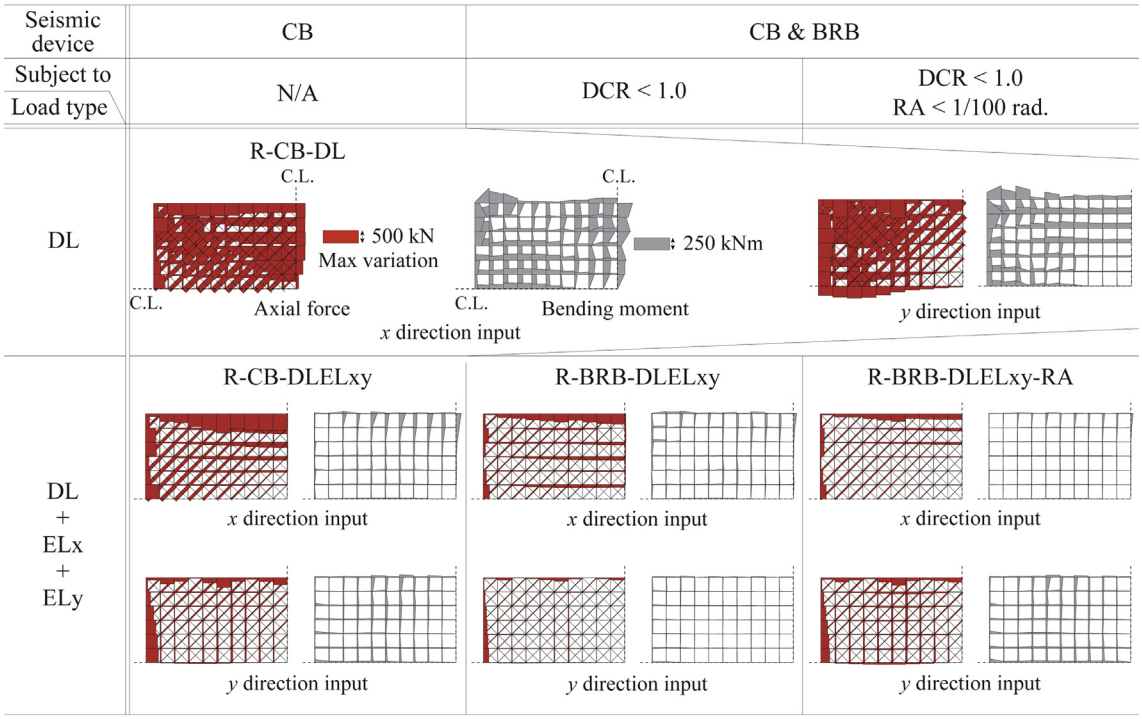

(b) Member force distribution by seismic response

Fig. 16. Member force distribution (GRSA and static analysis).

Table 6
Linear and approximate elasto-plastic buckling load factors.

Seismic device Subject to	CB N/A	CB & BRB DCR < 1.0	DCR < 1.0 & RA < 1/100 rad.
DL	52.87 → 10.57 (R-CB-DL)		
DL+ ELx	29.86 → 5.97 (R-CB-DLELx)	60.34 → 12.07 (R-BRB-DLELx)	28.16 → 5.63 (R-BRB-DLELx-RA)
DL+ ELy	23.26 → 4.72 (R-CB-DLELy)	55.50 → 11.10 (R-BRB-DLELy)	54.77 → 10.95 (R-BRB-DLELy-RA)
DL+ ELx+ ELy	35.32 → 7.06 (R-CB-DLELxy)	55.08 → 11.02 (R-BRB-DLELxy)	22.92 → 4.58 (R-BRB-DLELxy-RA)

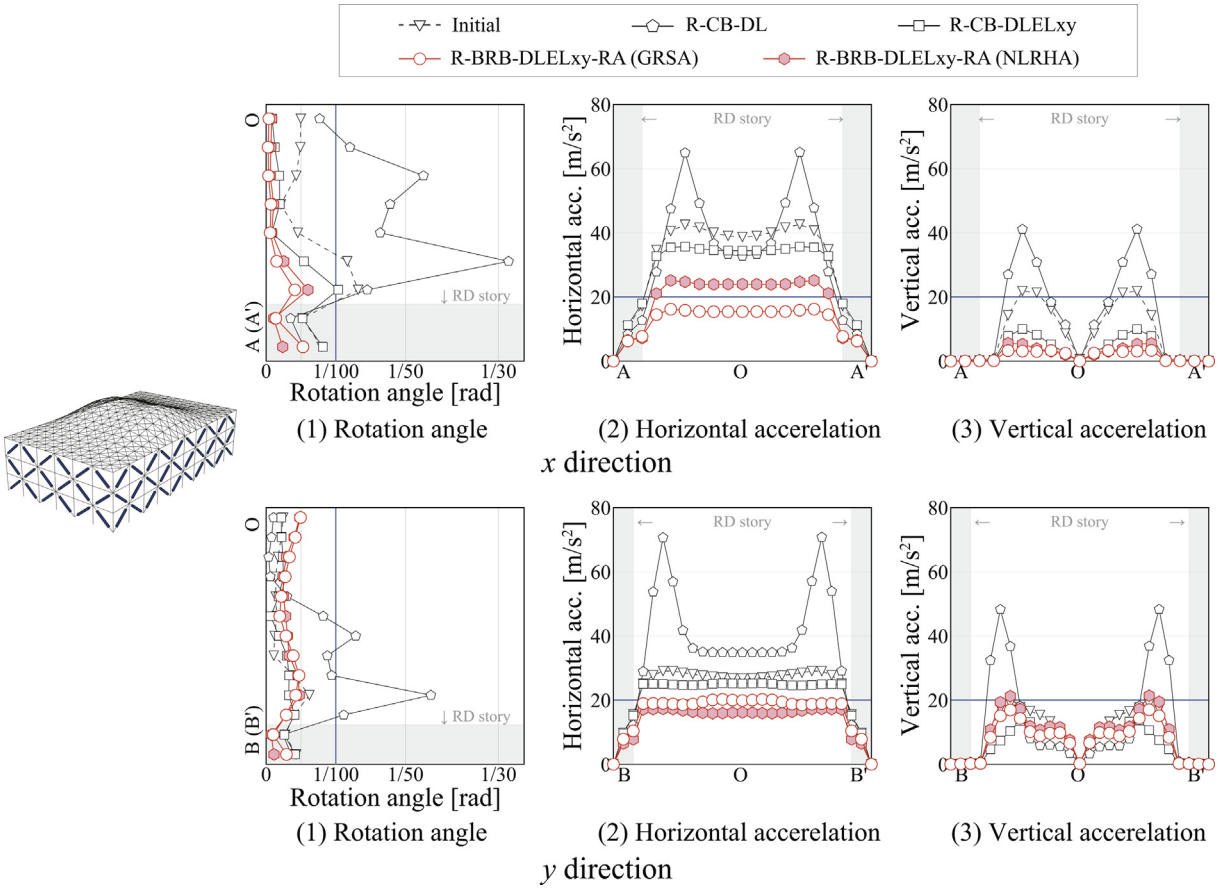

Fig. 17. Comparison of response from GRSAs and NLRHAs.

Table 7
Summary of computation time (Intel Core i9-7940X and DDR4 memory 64 GB).

Rectangular plan model (2070 DOFs) The number of seismic waves	3 waves DL + ELx, DL + ELy	6 waves DL+ ELx + ELy	1 wave DL + ELx, DL + ELy (Design spectrum)	2 waves DL + ELx + ELy (Design spectrum)
Converting design variables to 3DCADs Converting 3DCADs to FE models	45 *sec.*			
Performing 1GRSA	1.4 min.			
Performing GRSAs and static analysis	4.2 min.	8.4 min.	1.4 min.	2.8 min.
Calculating fitness	20 *sec.*	50 *sec.*	10 *sec.*	17 *sec.*
Subtotal time per generation	20 min.	35 min.	7 min.	12 min.
Total time (50 generations)	15 h.	27 h.	7 h.	10 h.

spectrum for decreasing the number of seismic waves. (b) to terminate the iteration based on the convergence of the objective function as shown in Section 2.4. (c) to increase the number of processors by using HPC [22,24,25,28,30] for reducing the computation time per iteration. As shown in Table 8, adopting solution (a), the total computation time was reduced to 7 to 10 h. Considering the objective functions converged in the 10th to 25th iteration in this paper, the time duration may be further reduced by half to one-third by adopting the solution (b). On the other hand, the time lost in the pre-and post-processing (constructing the 3DCAD models, conversion to the numerical models, and the computation of the objective functions) is also not negligible. Nevertheless, this time loss may be reduced by further optimizing the code.

5.3. Recommended use and limitations

Based on the application studies and the above discussion, the recommended procedure for GRSA-based computational morphogenesis is proposed in this section. Note that the initial shape of the structure and the specification of loads are assumed to be predetermined by the architect and/or engineer.

Step 1. Design the members of the initial structure against the service-level earthquake (or as per the selected country's design code e.g. [40]).
Step 2. Define the optimization problem. Determine the capacity range of adopted dampers placed in the supporting structure based on the design base shear against the design-

base earthquake. Provide additional constraints for the *z*-coordinates of the control points of NURBS as required by the architects if the initial shape is irregular. Assign the total strain energy of the roof members as the main objective function and the rotation angle *RA* as the constraint. The member length may also be assigned as a constraint to consider the allocation of finishing materials (if required). Assign only the design spectrum for seismic response evaluation in the fundamental design stage to reduce the total computation time, although a site-specific earthquake motion may also be used.

Step 3. Perform GRSA-based computational morphogenesis.

Step 4. Discuss the form-found geometry with architects and other members of the design team. Repeat Step 1 to Step 3 if other design options are desired.

Step 5. Perform NLRHA against specific earthquake motions on the final design option, and verify whether the seismic response demand satisfies the given design criteria. Finally, design the bracket (of the finishing material) based on the obtained acceleration response demands. Fine-tune and further proportion the member sections if required.

6. Conclusion

The following conclusions were obtained:

1) An efficient geometry of metal gridshell structures along with an efficient damper layout (that prevents member buckling and dropout of finishing materials) was obtained following the proposed optimization method.
2) According to the BRB layout optimization results, for a metal gridshell roof with a relatively heavy supporting structure with dampers, a larger BRB size is recommended to be placed on the lowest story (similar to a typical BRB proportioning for the design shear forces in multistory buildings).
3) A high-rise funicular geometry proved to be efficient in mitigating the member stress under dead loads, but the displacement and accelerations under the seismic loads were too large to guarantee structural safety and prevent the roof member from yielding or the dropout of finishing materials. In contrast, in a flattened roof geometry form-found considering the seismic loads, the horizontal sway vibration mode of the rigid body was predominant due to the improved dynamic stiffness, resulting in a reduced seismic response (within the acceptable range). According to the form-found roof shapes, an appropriate rise of the gridshell roof satisfying both the gravity and seismic demands lies in between the two shapes. However, as the precise geometry of the roof depends on the considered load combination, an optimal generalised shape (which is often sought by conventional methods of form-finding) for the roof against the dynamic loads could not be achieved.
4) GRSA evaluated the displacements of metal gridshell structures with sufficient practical accuracy. Although the nodal accelerations of the form-found roofs were smaller than those of the initial models, GRSA underestimated them by up to 0.8 g. NLRHA is therefore recommended to be performed on the final design model.
5) For a numerical model with around 2000 degree-of-freedoms, while one NLRHA on a single processor took 20 to 30 min to run, one GRSA took 1.4 to 1.7 min. Thus, GRSA significantly reduced the computation time for computational morphogenesis even while explicitly considering the complex dynamic response characteristics of gridshells. To further reduce the computation time, it is recommended to adopt only the design spectrum for the seismic input and terminate the iteration after the convergence of the objective function.

Disclosure

The authors have no conflicts of interest to declare.

Declaration of Competing Interest

The authors declare that they have no known competing financial interests or personal relationships that could have appeared to influence the work reported in this paper.

Acknowledgement

This work was supported by a Grant-in-Aid from the Japan Society for the Promotion of Science Fellowships (No. 21H04581).

References

[1] Ohmori H. Computational morphogenesis: Its current state and possibility for the future. Proceedings of the 6th International Conference on Computation of Shell and Spatial Structures. 2008.
[2] Adriaenessens S., Block P., Veenendaal D. and Williams C. (Eds).: Shell Structures for Architecture Form Finding and Optimization, Routledge, Oxon and New York, 2014.
[3] https://www.rhino3d.com/.
[4] http://bim-design.com/infra/product/dynamo/.
[5] International Association for Shell and Spatial Structures . Guide to Earthquake Response Evaluation of Metal Roof Spatial Structures. 2019.
[6] Takeuchi T, Terazawa T, Inanaga S, Matsui R. Collapse analysis of damaged space-frame gymnasiums in the 2016 Kumamoto Earthquake. Proceeding of the IASS Symposium 2018:2018.7.
[7] Terazawa Y, Inanaga S, Ryota M, Takeuchi T. Seismic damage evaluation of space frame roofs of RC gymnasiums. Journal of Structural and Construction Engineering (Transaction of AIJ) 2018;83(754):1789–99. https://doi.org/10.3130/aijs.83.1789.
[8] Nair D, Terazawa Y, Sitler B, Takeuchi T. Seismic response of long-span domes supported by multi-story substructures. Journal of the International Association for Shell and Spatial Structures 2020;61(2):140–57. https://doi.org/10.20898/j.iass.2020.204.007.
[9] Narita K, Terazawa Y, Matsui R, Takeuchi T. Response control of cantilevered RC walls in gymnasia with energy-dissipation roof bearing. Journal of Structural and Construction Engineering (Transaction of AIJ) 2015;80 (707):157–65. https://doi.org/10.3130/aijs.80.157.
[10] Narita K, Terazawa Y, Maehara K, Matsuoka Y, Matsui R, Takeuchi T. Dynamic loading tests and response evaluation of steel roof bearing with friction dampers. Journal of Structural and Construction Engineering (Transaction of AIJ) 2015;80(717):1717–25. https://doi.org/10.3130/aijs.80.1717.
[11] Block P, Lachauer M, Rippmann M. Thrust network analysis. Design of a cut-stone masonry vault, Shell Structures for Architecture Form Finding and Optimization, Routledge. Oxon and New York 2014:70–87.
[12] Marmo F, Rosati L. Reformulation and extension of the thrust network analysis. Comput Struct 2017;182(1):104–18. https://doi.org/10.1016/j.compstruc.2016.11.016.
[13] Michiels T, Adriaenssens S, Jorquera-Lucerga JJ. Parametric study of masonry shells found for seismic loading. Journal of IASS 2017;58(4):267–75. https://doi.org/10.20898/j.iass.2017.194.892.
[14] Michiels T, Adriaenssens S. Form-finding algorithm for masonry arches subjected to in-plane earthquake loading. Comput Struct 2018;195 (15):85–98. https://doi.org/10.1016/j.compstruc.2017.10.001.
[15] Michiels T, Adriaenssens S, Matthew D. Form finding of corrugated shell structures for seismic design and validation using non-linear pushover analysis. Eng Struct 2019;181:362–73. https://doi.org/10.1016/j.engstruct.2018.12.043.
[16] Tomasello G, Adriaenssens S, Gabriele S. Dynamic behavior of found shell structures according to modal and dynamic funicularity. Eng Struct 2019;198. https://doi.org/10.1016/j.engstruct.2019.109521.
[17] Shigeta Y, Kobayashi A, Minowa K, Ogawa T, Kato S. Optimization of shape and member stiffness distributions for single-layer reticulated shells of rectangular plan. Journal of the International Association for Shell and Spatial 2015;57 (4):173–86.
[18] Nascimbene R. Analysis and optimal design of fiber-reinforced composite structures: sail against the wind. Wind and Structures 2013.6,;16(6):541–60. https://doi.org/10.12989/was.2013.16.6.541.
[19] Linkwitz K. Force density method: design of a timber shell. Shell Structures for Architecture Form Finding and Optimization: Routledge, Oxon and New York; 2014. p. 59–71.

[20] Barnes MR. Form-finding and analysis of prestressed nets and membranes. Comput Struct 1988;30(3):685–95. https://doi.org/10.1016/0045-7949(88)90304-5.
[21] Terazawa Y, Takeuchi T. Generalized Response Spectrum Analysis for Structures with Dampers. Earthquake Spectra 2018. https://doi.org/10.1193/2F092217EQS188M.
[22] Terazawa Y, Takeuchi T. Optimal damper design strategy for braced structures based on generalized response spectrum analysis. Japan Architecture Review 2019:1–17. https://doi.org/10.1002/2475-8876.12122.
[23] Terazawa Y, Sano W, Takeuchi T. Design method of seismically isolated structures based on generalized response spectrum analysis. Journal of Structural and Construction Engineering (Transactions of AIJ) 2020;85(775):1187–97. https://doi.org/10.3130/aijs.85.1187.
[24] Terazawa Y, Takeuchi T. Elasto-plastic damper optimization routine for lattice towers based on generalized response spectrum analysis. Journal of the International Association for Shell and Spatial Structures 2018;59(4):243–50. https://doi.org/10.20898/j.iass.2018.198.035.
[25] Terazawa Y, Fujishima M, Takeuchi T. Optimal mixed placement and capacity distribution of buckling-restrained braces and conventional braces on a large metal spatial structure without rigid diaphragm assumption. Frontiers in Built Environment 2022;8. https://doi.org/10.3389/fbuil.2022.954117.
[26] Asai T, Terazawa Y, Miyazaki T, Lin PC, Takeuchi T. First mode damping ratio oriented optimal design procedure for damped outrigger systems with additional linear viscous dampers. Engineering Structures 2021:247. https://doi.org/10.1016/j.engstruct.2021.113229.
[27] Terazawa Y, Ishibashi S, Omura H, Asai T, Takeuchi T. Non-linear Dynamic Response Characteristic of Single-Damped Outrigger Systems with Oil Dampers or Elasto-plastic Dampers Considering Design Earthquake Levels. Journal of Structural and Construction Engineering (Transaction of AIJ) 2022;87(791):149–60. https://doi.org/10.3130/aijs.87.149.
[28] Ishibashi Y, Terazawa Y, Tanaka H, Yokoyama R, Mizuno Y, Takeuchi T. A novel damped braced tube system for tall buildings in high seismic zones. The Structural Design of Tall and Special Buildings 2022;2:e1926. https://doi.org/10.1002/tal.1926.
[29] Terazawa Y, Ishibashi Y, Tanaka H, Yokoyama R, Mizuno Y, Takeuchi T. Numerical investigation of dynamic characteristic of damped braced tube system with different damped slit configuration. Journal of Structural and Construction Engineering (Transaction of AIJ) 2022;87(802):1247–56. https://doi.org/10.3130/aijs.87.1247.
[30] Terazawa Y, Tanaka H, Takeuchi T. Optimal seismic response control of damped braced tube system with focus on cost performance of introducing energy-dissipation devices. Journal of Structural and Construction Engineering (Transaction of AIJ) 2022;87(801):1082–92. https://doi.org/10.3130/aijs.87.1082.
[31] Sinha R, Igusa T. CQC and SRSS methods for non-classically damped structures. Earthquake Eng Struct Dyn 1995;24:615–9. https://doi.org/10.1002/eqe.4290240410.
[32] The Japan Society of Seismic Isolation. Manual for Design and Construction of Passively - Controlled Building third Edition. Daioh Co., Ltd. 2013. in Japanese.
[33] Takeuchi T, Wada A. Buckling-restrained braces and applications. The Japan Society of Seismic Isolation; 2017.
[34] Gu Q, Zona A, Peng Y, Dall'Asta A. Effect of buckling-restrained brace model parameters on seismic structural response. Journal of Constructional Steel Research 2014;98:100–13. https://doi.org/10.1016/j.jcsr.2014.02.009.
[35] Castaldo P, Tubaldi E, Selvi F, Gioiella L. Seismic performance of an existing RC structure retrofitted with buckling restrained braces. Journal of Building Engineering 2021;33:. https://doi.org/10.1016/j.jobe.2020.101688101688.
[36] Castaldo P, Amendola G. Optimal DCFP bearing properties and seismic performance assessment in nondimensional form for isolated bridges. Earthquake Eng Struct Dyn 2021;50(9):2442–61. https://doi.org/10.1002/eqe.3454.
[37] Kitayama S, Constantinou MC. Collapse performance of seismically isolated buildings designed by the procedures of ASCE/SEI 7. Eng Struct 2018;164:243–58. https://doi.org/10.1016/j.engstruct.2018.03.008.
[38] Castaldo P, Amendola G. Optimal sliding friction coefficients for isolated viaducts and bridges: A comparison study. Structural Control and Health Monitoring 2021:e2838.
[39] Kitayama S, Constantinou MC. Probabilistic seismic performance assessment of seismically isolated buildings designed by the procedures of ASCE/SEI 7 and other enhanced criteria. Eng Struct 2019;179:566–82. https://doi.org/10.1016/j.engstruct.2018.11.014.
[40] Ministerial Notification No. 1461 of the Ministry of Construction, Japan, 2000.
[41] The Ministry of Construction of Japan. Commentary of the technical background about the regulations of the revised Japanese Building Law. Gyousei. 2001. in Japanese.
[42] Architectural Institute of Japan. AIJ Standard for Allowable Stress Design of Steel Structures. 2019. in Japanese.
[43] And SLC, Hanaor A. Force limiting devices in space trusses. Journal of the Structural Division, Journal of the Structural Division 1979;105(5):939–51.
[44] International Association of Shell and Spatial Structures. Guide to Buckling Load Evaluation of Metal Reticulated Roof Structures. 2014.